

Mapping Tropical Dry Miombo Woodlands into Functional Forest Classes Using Sentinel-1 and Sentinel-2 Imagery and Machine Learning

Kennedy Kanja, Ce Zhang, Melvin Lippe and Peter M. Atkinson

Abstract

Tropical dry forests, such as the Miombo woodlands, play crucial roles both as an effective global carbon sink, and as the source of livelihood for a vast number of local communities. However, mapping Miombo woodlands accurately into definable classes is a great challenge due to their sparse and heterogeneous nature and their alteration due to anthropogenic impacts. Nevertheless, such mapping is important to underpin management and conservation efforts. We explored the potential of Sentinel (S-1) and Sentinel-2 (S-2) seasonal and multi-seasonal images for two tasks: (i) mapping Land Use Land Cover (LULC) such as to identify the Miombo woodlands and (ii) mapping three specific forest classes (reference, degraded and regrowth forests) *within* the Miombo woodlands of Zambia. The Random Forest (RF) algorithm within Google Earth Engine (GEE) was selected for the LULC classification while a U-Net convolutional neural network (CNN) was applied to classify the different types of forest. Models were trained, validated, and tested using ground validation data. The RF model achieved an overall accuracy of 93% for LULC classification, with the forest class F1-scores ranging from 93% to 96% across different seasons. The U-Net CNN effectively delineated the Miombo woodlands into reference, degraded and regrowth forests, with respective F1-scores of 85%, 73% and 72%. Combining multi-seasonal S-1 and S-2 images and their derivatives yielded the greatest accuracy for LULC mapping, while combining the year-round S-1 and S-2 bands produced the highest F1-scores for the forest type classification. The hierarchical approach employed was, thus, demonstrated to be effective, providing more nuanced functional forest information. The approach holds great promise for mapping and monitoring programs aiming to manage and conserve the Miombo woodlands sustainably.

Keywords: deep learning, forest type; google earth engine; hierarchical, LULC; Miombo woodlands; optical; SAR; tropical dry forests.

1. Introduction

Tropical dry woodlands represent a sink to terrestrial carbon and a source of livelihood for local communities, amongst many other ecosystem services and, therefore, need to be managed sustainably. However, less research exists on mapping tropical dry forests compared to tropical moist forests such as the Amazon rainforest (David et al., 2022). The Miombo woodlands are a typical tropical dry woodland found extensively in Southern and Eastern Africa. They extend across the Democratic Republic of Congo (DRC), Angola, Mozambique, Malawi, Tanzania, Zimbabwe and Zambia (Kamusoko et al., 2014). These tropical dry woodlands, while important, are challenging to classify into easily definable functional forest types due to their complex vegetation composition and patterns (Ribeiro et al., 2012; Day et al., 2014). Moreover, constant human use coupled with the impact of fire has led to fragmentation of the Miombo vegetation structure and distribution.

There exists a pressing need for methods and algorithms that can map tropical dry forest types accurately. Discrimination of the different forest types is important for accurate monitoring and reporting of above ground biomass, especially as most of the countries in which the Miombo woodlands are found are domesticating global efforts such as REDD+, NDCs and the Bonn Challenge aimed at sustainable forest management (Shamaoma et al., 2022; David et al., 2022). Useful Miombo forest types to discriminate include intact, degraded or disturbed, and regrowth forests. These forest types differ in the ecosystem services that they provide as well as the amounts of above ground biomass they store (Solórzano et al., 2021).

Improvements in the classification of these forest types is, thus, needed to support more accurate estimation of above-ground biomass and to underpin evidence-based forest policies and management strategies to mitigate deforestation and its effects.

Several studies on land use and land cover (LULC) and vegetation type mapping for the Miombo woodlands and other forest biomes were carried out with Landsat-8, with high accuracies achieved (Mayes et al., 2015; Connette et al., 2016; Halperin et al., 2016; Phiri et al., 2018; John et al., 2021). However, Landsat-8 with a spatial resolution of 30 m is more prone to mixed pixels compared to Sentinel-2 (S-2) with a spatial resolution of 10 m (visible and near infrared bands), considering the heterogeneity of the Miombo woodlands in terms of both composition and pattern. Romijn et al. (2015) proposed the use of finer spatial resolution remote sensing data for accurate mapping of dry woodlands such as the Miombo due to their open and sparse structure, and history of human impacts. Studies based on S-2 reported increases in the accuracy of LULC and forest mapping (Adagbasa et al., 2019; Mudereri et al., 2021). For example, Puletti et al. (2018) used S-2 for forest classification in a Mediterranean environment to map forest type (beech forests, mixed spruce-fir forests, chestnut forests and mixed oak forests) and to discriminate forest categories (conifer, broadleaved and mixed forest) and obtained an overall accuracy of >83%. However, David et al. (2022) found no published research that used S-2 to map Miombo woodland LULC and forest type.

Studies that used Synthetic Aperture Radar (SAR) data alone (McNicol et al., 2018; Ngo et al., 2020; Prudente et al., 2020) and in combination with optical data (Carreiras et al., 2017; Brandt et al., 2018; Lu Zhang, 2019; Mercier et al., 2019) have received much attention because the synergy of optical and SAR data is reported to increase the accuracy of LULC and vegetation mapping. According to David et al. (2022), few research papers were published mapping the Miombo woodlands using SAR and optical data, and even less so using Sentinel-1 (S-1) and S-2. Our review of the literature indicated very few research publications in which the effects of seasonal and temporal variation on mapping LULC and vegetation types using S-1 and S-2 were explored (Altarez et al., 2023). The current research is intended to bridge these research gaps.

Machine learning classifiers such as the random forest (RF), extreme gradient boosting (XGBoost) and support vector machines (SVM) have been used extensively for LULC and vegetation type mapping (Ngo et al., 2020; John et al., 2021; Mudereri et al., 2021). Cloud-based computing using Google Earth Engine (GEE) can facilitate mapping large areas due to its ability to handle large datasets (Tsai et al., 2018; Praticò et al., 2021). The past few years have seen U-net, a convolutional neural network-based form of deep learning, become prominent for LULC and forest type classification due to its capability to learn spatial context, unlike other machine learning methods that rely on already-made context features (Kattenborn et al., 2021). The fully-convolutional neural network, U-Net, can classify pixels by identifying patterns in an image using both spectral and spatial domains without sacrificing spatial resolution (Solórzano et al., 2021). Several studies have used the state-of-the-art U-Net for forest mapping (Solórzano et al., 2021; Dal Molin and Rizzoli, 2022; Altarez et al., 2023). However, we found no studies that utilized GEE and U-net for mapping the Miombo woodlands, a major component of the world's tropical dry woodlands biome.

To the best of our knowledge, no study has explored seasonal S-1 and S-2 images, and their derivatives, for LULC mapping of the Miombo woodlands using the GEE platform. Further, no study used the U-net algorithm to map the forest types that characterise the Miombo woodlands using S-1 and S-2 imagery. This research aimed to explore the use of S-1 and S-2 seasonal and multi-seasonal (i.e., including all seasonal mean images for rainy, dry, and hot seasons stacked) images for LULC mapping using RF within GEE, and to test the capability of U-net to discern forest patterns and, thus, effectively classify Miombo forest types (reference, degraded and regrowth). Our proposed approach is hierarchical in that we first identify Miombo forest areas through LULC classification within GEE to create a forest mask, and then use the U-Net deep learning algorithm to discriminate between the forest types. We hypothesised that this approach would produce accurate forest type maps which can be used for further applications such as for forest conservation initiatives and to increase the accuracy of AGB mapping for REDD+ projects, which is urgently needed. The remainder of this research is arranged as follows; description of the study areas and the datasets used; experimental design and methodology; results; discussion; conclusion.

2. Methodology

In this section, the hierarchical classification methodological framework is presented. We first describe the study area and data acquisition in sections 2.1 and 2.2, respectively. In section 2.3, we explain the design of the experiments conducted in this research. In sections 2.4 and 2.5 we describe the pre-processing of the data through visualisation and the hierarchical classification analysis, respectively. In section 2.6 we discuss the quality assessment of the results. Fig. 1 shows the methodological framework.

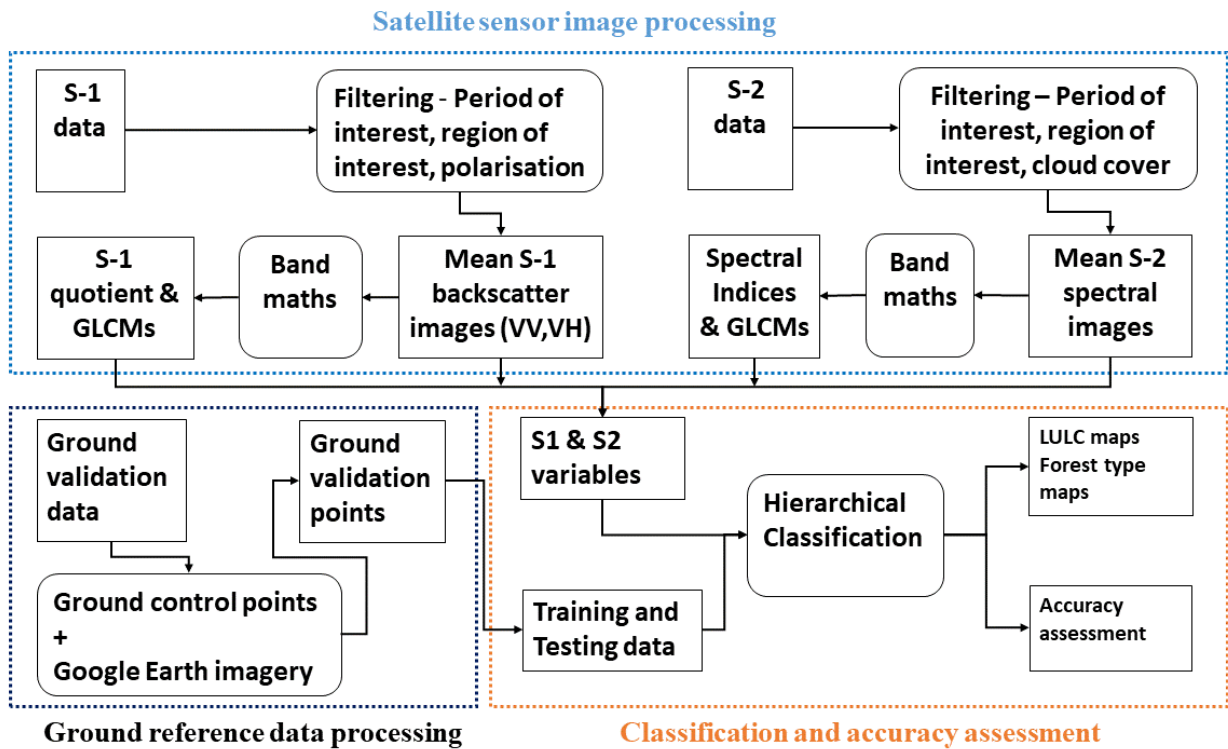


Fig. 1. Flowchart showing the methodology followed in this research.

2.1. Study Area

This research used data collected across 12 landscapes encompassing the Miombo woodlands of Zambia through the research project Landscape Forestry in the Tropics (LaforeT: <http://www.la-foret.org/>). These landscapes are spread across Zambia's Miombo woodlands covering three provincial administrative boundaries with each province depicting a different deforestation context (initial, middle and advanced), based on national and international forest reports (Velasco et al., 2022). The landscape tiles were created across six districts, with two districts in each province, and every district having two landscape tiles (Fig. 2). The districts were Nyimba and Petauke from Eastern province, Masaiti and Lufwanyama from Copperbelt province, and Mufumbwe and Mwinilunga from North-western Province. All 12 landscapes are multi-functional with a great diversity of LULC types and forest types. We chose to use the LaforeT landscapes for Zambia because (1) they encompass both dry and wet Miombo woodlands and, thereby, facilitate a balance for model training and (2) the ground validation exercise was extensive ($n=3,000$) and explicit in defining the classes of interest for the current research.

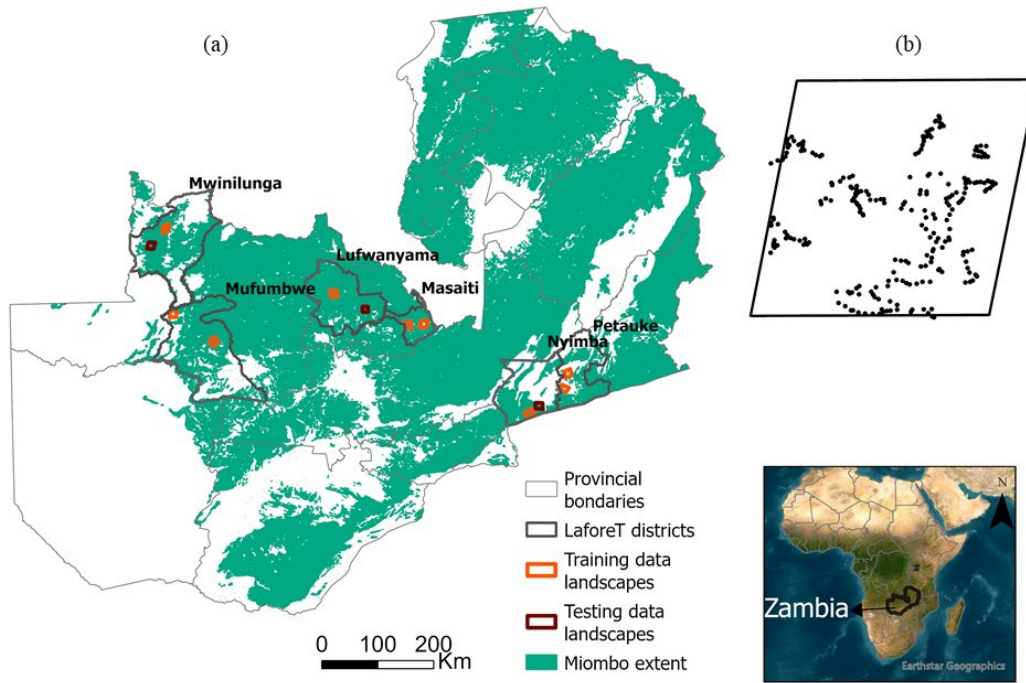


Fig. 2. Map of the study areas showing (a) the extent of the Miombo woodlands in Zambia, the provincial and LaforeT district boundaries and the location of the training and validation landscape tiles and (b) one zoomed-in landscape tile showing the ground validation data points.

2.2. Data Acquisition

2.2.1. Satellite sensor imagery

We used Sentinel-1 (S-1) and Sentinel-2 (S-2) images for the current research. Using GEE, we downloaded S-2 L2A images for the year 2019 to conform to the ground dataset collection period. Similarly, we downloaded S-1 Ground Range Detected (GRD) scenes from ESA's S-1 satellites (A and B) that use dual polarization C-band Synthetic Aperture Radar (SAR).

We composited freely available S-1 SAR images and S-2 optical images using code in GEE developed elsewhere (Tassi et al., 2021; Vizzari, 2022). A collection of cloud masked S-2 L2A images was made by filtering for our study area and for the four primary periods of interest (rainy season, dry season, hot season and year-round), applying a median reduction for all available images. Ten S-2 bands (band 2 to band 8A, band 11 and band 12) were targeted, and resampled to a spatial resolution of 10 m to conform to the spatial resolutions of the RGB and NIR bands. We also computed and added to the original bands six vegetation indices namely the Normalized Difference Vegetation Index (NDVI), Enhanced Vegetation Index (EVI), Normalized Difference Moisture Index (NDMI), Normalized Difference Water Index (NDWI), Bare Soil Index (BSI) and Shadow Index (SI). The NDVI and EVI are commonly used for LULC mapping, given their capability to quantify vegetation greenness (Phiri et al., 2018; Mercier et al., 2019). The NDMI and NDWI are normalised indices like the NDVI, but use the shortwave infrared and green bands, respectively. Both are used for identifying vegetation water content and water bodies, respectively (Adagbasa et al., 2019; Decuyper et al., 2022). The BSI distinguishes bare soil from other LULC classes while the SI is used in forestry and crop mapping (Vizzari, 2022).

A similar approach of filtering by study area, period of interest, instrument mode (IW) and polarisation (VH and VV) was applied to the S-1 datasets. S-1 bands VV and VH were downloaded with a spatial resolution of 10 m.

The GLCM algorithm in GEE was utilized to compute the texture metrics with input gray-level images generated using eqs. (1) and (2) for S-2 and S-1, respectively with a window size of 2 pixels. The input bands and the window size used in this research follow the approach of Tassi et al. (2021). The weights in eq. (1) are standard weights mapping RGB to greyscale. Although originally designed based on how sensitive the human eye is to different colours in visible light, the weights can be adapted when the Red band is substituted with the NIR band (Tassi et al., 2021; Vizzari, 2022). Texture information is used in most studies to increase the accuracy of forest type mapping (Numbisi et al., 2019; Ferrer Velasco et al., 2022). Five texture metrics (angular second moment, contrast, correlation, variance and inverse difference moment) were selected for both S-1 and S-2.

$$\text{S-2 Gray-level Image} = (0.3 * \text{NIR}) + (0.59 * \text{RED}) + (0.11 * \text{GREEN}) \quad (1)$$

$$\text{S-1 Gray-level Image} = (\text{VH} - \text{VV}) / (\text{VH} + \text{VV}) \quad (2)$$

2.2.2. Ground reference data

We used ground data collected under the LaforeT project for Zambia (Ferrer et al., 2023). A total of 3,000 ground validation points (GVPs) capturing the main LULC types (Forest, 1,601; cropland, 629; settlements, 265; grassland, 187; other land, 161; wetlands, 157 GVPs) were collected across the 12 landscapes that formed the LaforeT research sites for Zambia. LaforeT applied a stratified sampling approach to capture the main forest and LULC types in each of the 12 landscapes. Ground data collection was conducted between April 2018 to October 2019. Details on the ground data collection procedure can be found in (Velasco et al., 2022). The original LaforeT GVPs classes were realigned to conform to the Inter-Governmental Panel on Climate Change (IPCC) classes, namely forests, cropland, grassland, wetlands, other land, and settlements. We used Google Earth Pro fine-resolution and S-2 images to recheck these points as well as to populate the LULC classes that were less commonly represented such as wetlands, settlements, and other land.

2.3. Experimental Design

We designed experiments to compare the accuracies of the LULC classification and forest type classification when using various dataset combinations (Table 1). In total, 28 variables were extracted. Ten raw bands were derived from the S-2 bands, two raw bands from the S-1 bands, 10 texture metrics from both the S-1 and S-2 bands, and six vegetation indices from the S-2 bands. These variables were chosen based on previous, similar studies (Mercier et al., 2019; Lopes et al., 2020; Mudereri et al., 2021; Vizzari, 2022). The LULC classification experiments made use of all 28 extracted variables while the forest type classification experiments used only the raw bands from S-1 and S-2.

Table 1

Experimental design to compare the accuracies of the LULC classification and forest type classification when using S-1 and S-2 bands and their derived indices.

Sensor	Time period	Dataset combination	Number of experiments
S-1	Rainy	S-1 bands S-1 textures S-1 bands + textures	12-LULC
	Dry		4-Forest types
	Hot		
	Annual		
S-2	Rainy	S-2 bands	12-LULC
	Dry	S-2 textures	4-Forest types
	Hot	S-2 bands + textures	

	Annual	
S-1 + S-2	Rainy	5-LULC
	Dry	4-Forest types
	Hot	S-1 bands + S-1 textures + S-2 bands + S-2 textures + S-2 vegetation indices
	Annual	
	Multi-seasonal	

2.4. Data visualisation

As part of preparing the training data, we generated spectral and backscatter profiles that represented the mean spectral reflectance and mean backscatter for each of the LULC and forest type points (with a buffer of 15 m) and polygons, respectively, for the S-1 and S-2 bands. This was done to visually assess the separability of our training data. We also performed explanatory data analysis by summarising and graphically visualising the data to check for correlations, any unusual anomalies or outliers, and to identify the distributions. This informed the selection of combinations of remote sensing variables during the classification experiments.

2.5. Classification algorithms

2.5.1. RF for LULC classification

The RF algorithm was selected for this research based on its ability to produce high LULC accuracies, especially when working with large datasets and training samples (Kamusoko et al., 2014; Phiri et al., 2018; Solórzano et al., 2021; Tassi et al., 2021; Velasco et al., 2022). The RF algorithm is an ensemble machine learning method which uses decision trees to train on random subsets of the observed and predictive variables and then assigns a class to each pixel having the most votes from the individual trees (Breiman, 2001). The IPCC classes were the official classes used for forest monitoring and reporting in our study area and were, therefore, chosen for this study, facilitating easier comparison of the results with those of other similar studies and secondary data sources. The RF classifier was trained using 70% randomly selected points from all the ground validation points and validated using the remaining 30%. The training and validation subsets were maintained for all the LULC classification experiments conducted in this research, thus, providing effective comparability within the experiments. All the classification experiments were carried out in GEE.

2.5.2. U-net for Forest type classification

We tested the potential of the state-of-the-art U-net CNN to effectively delineate the three forest classes of interest in the Miombo woodlands (reference, degraded forests and regrowth forests). For the purposes of this research, and as adopted by the ground data collectors, the definitions of the three forest types used are as follows:

1. **Reference (intact) forest** refers to a forest that has little or no disturbance with a tree composition of mostly mature old-growth forests or intact primary forests and secondary forests with the last disturbance at least 10 years ago, without undergoing clear felling,
2. **Degraded forest** represents areas with a more recent disturbance of not more than 10 years (mostly human impact in the form of logging for timber, firewood, etc.), leading to a current state of degradation or a reduction of forest canopy cover, but not completely clear felled,
3. **Regrowth forest (secondary forest)** includes those forested areas that were at one point completely clear felled and converted to other LULCs, or in some cases with few trees left standing as a result of shifting cultivation or charcoal burning, but which have subsequently undergone, or are currently undergoing, a recovery process (Fig. 3).

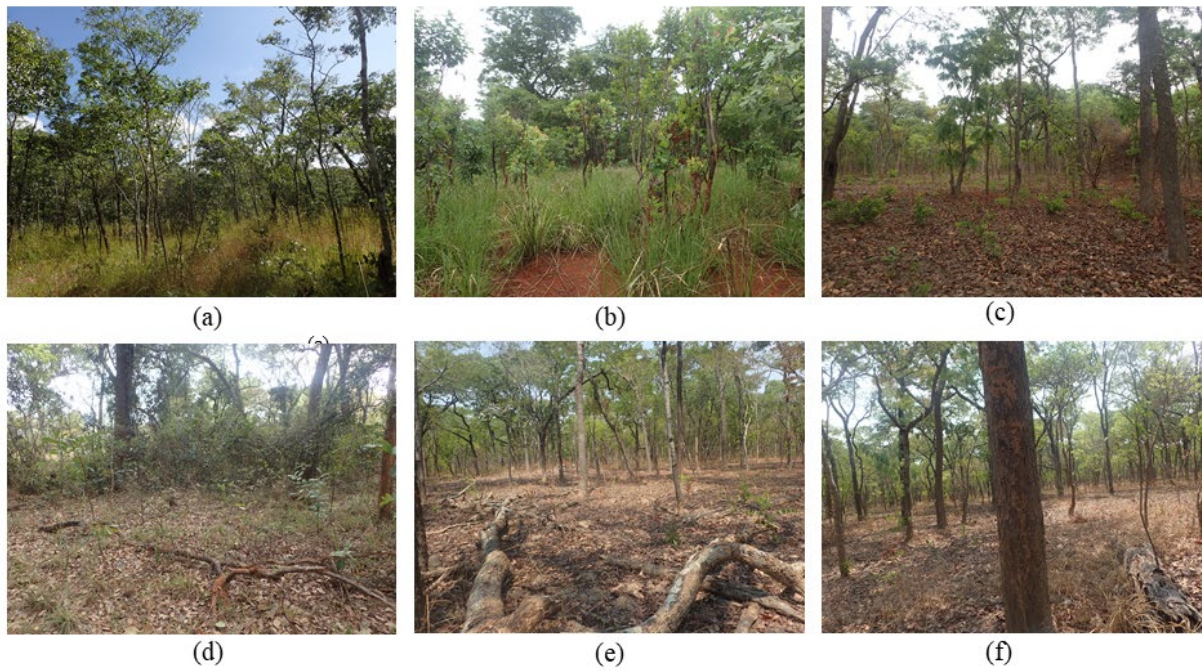


Fig. 3. Photographs depicting forest types in the Miombo woodlands. (a, b) Regrowth, (c, d) Degraded, (e, f) Reference (intact).

The U-net model classifies images per-pixel by assigning each pixel to a particular class. Recently, several studies used U-net to conduct various forest classification tasks obtaining very high accuracies (Wagner et al., 2019; Isaienkov et al., 2021; Hamedianfar et al., 2022; Altarez et al., 2023).

As noted by (Hamedianfar et al., 2022) in their review of deep learning for forest applications, it can be laborious to prepare annotations for training a CNN architecture. This is of particular relevance, because to-date little research exists on mapping forest types amongst Zambia's Miombo woodlands, and this makes it challenging to find a readily available dataset with which to train the models. Hence, we relied on the 1600 GVPs for forest type and very fine resolution images in Google Earth Pro and S-2 images to digitise 600 forest type polygons (Table 2). We created 664 systematically selected 64×64 pixel tiles across the 12 landscapes encompassing the 600 digitised forest type polygons. We masked out non-forest pixels based on our LULC classification and visually classified the remaining forest pixels into reference, degraded and regrowth forests using the forest type polygons and Google Earth Pro. This data preparation approach for deep learning was adopted from previous research (Solórzano et al., 2021; Isaienkov et al., 2021; Altarez et al., 2023). The 664 tiles with a spatial resolution of 10 m were converted to polygons and used for training, validation and testing of U-Net (Bragagnolo et al., 2021). One landscape from each of the study regions was selected randomly and reserved for model testing, while the rest of the landscapes were used for model training.

Table 2

The number of digitised polygons and their area per forest type.

Class	Digitized polygons	Area (ha)
Reference (intact)	56	870
Degraded	387	1431
Regrowth	157	144

2.6. Quality analysis

To assess classification accuracy, we compared our maps with two secondary maps, the integrated land use assessment (ILUAI) national maps for Zambia (Shakachite et al., 2016) and the ESRI land cover maps (<https://livingatlas.arcgis.com/landcover/>). The LULC accuracy assessments were evaluated using a confusion matrix in GEE where the number of correctly classified LULC pixels was measured from the validation dataset. For the forest type U-net models, we selected the best models based on the results of model validation in the form of Precision (also known as user's accuracy, eq. 3), Recall (also known as producer's accuracy, eq. 4) and F1-score (eq. 5) (Wagner et al., 2019). The most accurate U-net models were then tested on an independent dataset reserved during data preparation. Again, we created a confusion matrix from the classified maps. Fine spatial resolution Google Earth images were consulted as a secondary source of reference information. From the confusion matrix we were able to calculate thematic accuracy measures such as the overall accuracy (OA, eq. 6), user's accuracy (UA) and producer's accuracy (PA), as well as the Kappa statistic (K , eq. 7) (Solórzano et al., 2021). Qualitative assessment on the classified maps was also explored through visual inspection. In addition, we used the z -test statistic to test for significant differences between the classification results from the various data combinations.

$$\text{Recall (PA)} = \frac{\text{Number of correctly identified pixels in a given map class}}{\text{Number claimed to be in that map class}} \quad (3)$$

$$\text{Precision (UA)} = \frac{\text{Number of correctly identified pixels in a given map class}}{\text{Number actually in that reference class}} \quad (4)$$

$$\text{F1-score} = 2 * \frac{\text{Precision} * \text{Recal}}{\text{Precision} + \text{Recal}} \quad (5)$$

$$\text{Overall accuracy (OA)} = \frac{\text{Number of correct predictions}}{\text{Total number of predictions}} \quad (6)$$

$$\text{Kappa statistic (K)} = \frac{\text{Observed agreement} - \text{Expected agreement}}{1 - \text{Expected agreement}} \quad (7)$$

3. Results

3.1. Data visualisation

For S-1 bands we noted different class separability based on VV and VH radar backscatter between the three considered seasons, with the rainy season producing a greater separation between all classes except for cropland and settlements. The dry season produced clear separability using both VV and VH backscatter for the six LULC classes. The hot season also produced a clear separation of the classes except for cropland and grassland in VV backscatter and cropland and other land in VH backscatter (See Supplementary Fig. S1). The largest backscatter values were observed for the forest class followed by built-up using both VV and VH backscatter. This result is expected because radar backscatter is known to interact with forest crowns, branches and trunks, and buildings, resulting in single, double, and triple bounces. These findings are consistent with those of others (Nicolau et al., 2021; Altarez et al., 2023). For the forest type classes, (See Supplementary Fig. S2), radar backscatter in VH resulted in more distinct classes, especially for the rainy and hot seasons, although clear separation is visible, even in VV backscatter, with close similarities for the degraded and regrowth classes, while the reference forest class stands out, similar to Verhegghen et al. (2022).

The analysis of spectral reflectance patterns across S-2 bands showed that the separability of the six IPCC land cover classes and forest type classes varied notably by season. For the rainy season, all the IPCC classes were only narrowly separated in the Red (B4), Near Infrared (NIR, B5), and Red Edge (B7) bands with the

SWIR bands producing a clear separation between all classes, except for forest and grassland, while the forest type classes regrowth and degraded were indistinguishable across all the bands (see Supplementary Fig. S3). For the dry season, the six IPCC classes were visibly well separated in the Red Edge bands (B6 to B8A) and the Shortwave Infrared bands, while for the forest types there was no visible separation between regrowth and degraded forests in the visible and SWIR bands, and no observable separation between regrowth and reference forests in the Red Edge (B6 to B8A) and NIR bands (see Supplementary Fig. S4). For the hot season, visible separation between the IPCC classes was evident in the Red (B4), Red Edge (B5), and SWIR bands, while forest types remained barely separable in the SWIR bands especially between the degraded and regrowth classes (see Supplementary Fig. S5). For the year-round (i.e., annual mean) imagery, IPCC classes were visibly separable across all Red Edge bands (B6, B7, B8A), NIR, and SWIR-2 bands, while forest type classes also demonstrated visual separation in the Red (B4), Red Edge (B5) and SWIR bands (see Supplementary Fig. S6). These observed reflectance patterns are consistent with those reported by Altarez et al. (2023). Note that the figures referred to are based on mean spectral reflectance values for the purposes of visual interpretation and, thus, provide only an indication of *potential* separability, ignoring within-class variation.

3.2. Comparison between S-1 SAR and S-2 optical imagery for LULC mapping

3.2.1. Model overall accuracies

The results revealed a significant difference between the classification accuracy using S-1 SAR data and S-2 optical data. We conducted z-test statistics at the 5% level of significance. The *p*-values obtained when we compared the classification accuracies using the S-1 and S-2 bands singly, as well as their combination with GLCM textures, were highly significant (*p*-values < 0.001). The highest overall accuracies and Kappa indices were obtained using S-2 bands and textures combined (Table 3).

Using the S-2 bands alone produced overall accuracies and Kappa indices that were evidently superior to the overall accuracies and Kappa indices for the S-1 bands. For the S-2 bands alone, and combined with textures, the highest overall accuracy and Kappa index were obtained for the rainy season followed by the hot season, with the lowest accuracy in the dry season. Using the S-1 bands alone produced the highest overall accuracy for the hot season followed by the rainy season and with the lowest accuracy in the dry season. A similar pattern was seen when the S-1 bands were combined with their textures, where the overall accuracies for the hot season and rainy season were similar, and higher than for the dry season. This result agrees with our interpretation of the backscatter and spectra.

We observed that using the bands alone produced greater accuracy than using the textures alone for both the S-1 and S-2 datasets. Overall, our results comparing SAR and optical data are similar to those for other studies that compared S-1 and S-2 for LULC mapping (Mercier et al., 2019; de Souza Mendes et al., 2019; Lopes et al., 2020).

Table. 3

LULC overall accuracies and Kappa indices for S-1 and S-2 data comparisons.

	Overall Accuracy (%)				Kappa Index (%)			
	Rainy	Dry	Hot	Year-round	Rainy	Dry	Hot	Year-round
S-1 Bands	67.8	64	70	71.9	48	42	51	54.3
S-2 Bands	87.2	84	86	85.4	80.4	75	78	77.3
S-1 Textures	57.7	57	55	57.7	25	25	15	26.4
S-2 Textures	81.3	81	78	81	71.2	71	66	66.5

S-1 Bands & Textures	73.5	69	74	77.8	57.8	49	57	64.2
S-2 Bands & Textures	89.1	87	88	88.7	83.2	80	81	82.5

3.2.2. Class F1-scores

Using the S-1 bands alone, and combined with their texture bands, is almost as accurate as using the S-2 bands alone, and combined with their texture bands, for forest class mapping (Fig. 4). We noted that the S-1 bands alone contributed more to increasing forest mapping accuracy than the S-1 textures when the two were combined. This was also noted for the other classes except for settlements where S-1 texture bands were more accurate than the S-1 bands (Fig. 4). Overall, the S-2 bands alone and combined with their texture bands, produced the highest F1-scores across the four time periods for forest mapping. Cropland was easily detectable in the rainy season with the highest F1-score of 83.9% (See Supplementary Table S1). The highest F1-score for mapping grassland was produced in the rainy season. S-1 images produced low F1-scores for grasslands with the highest F1-score in the rainy season. The highest F1-score for settlements was produced in the rainy season using S-2 bands and textures. For other land the highest accuracy was produced in the dry season with S-2 bands alone (See Supplementary Table S2). Wetlands were fairly well classified in all three seasons using both the S-1 and S-2 images. We found that S-1 produced a low accuracy for classes where backscatter interaction is poor such as other land, cropland and grassland; a similar result reported by other researchers (Prudente et al., 2020).

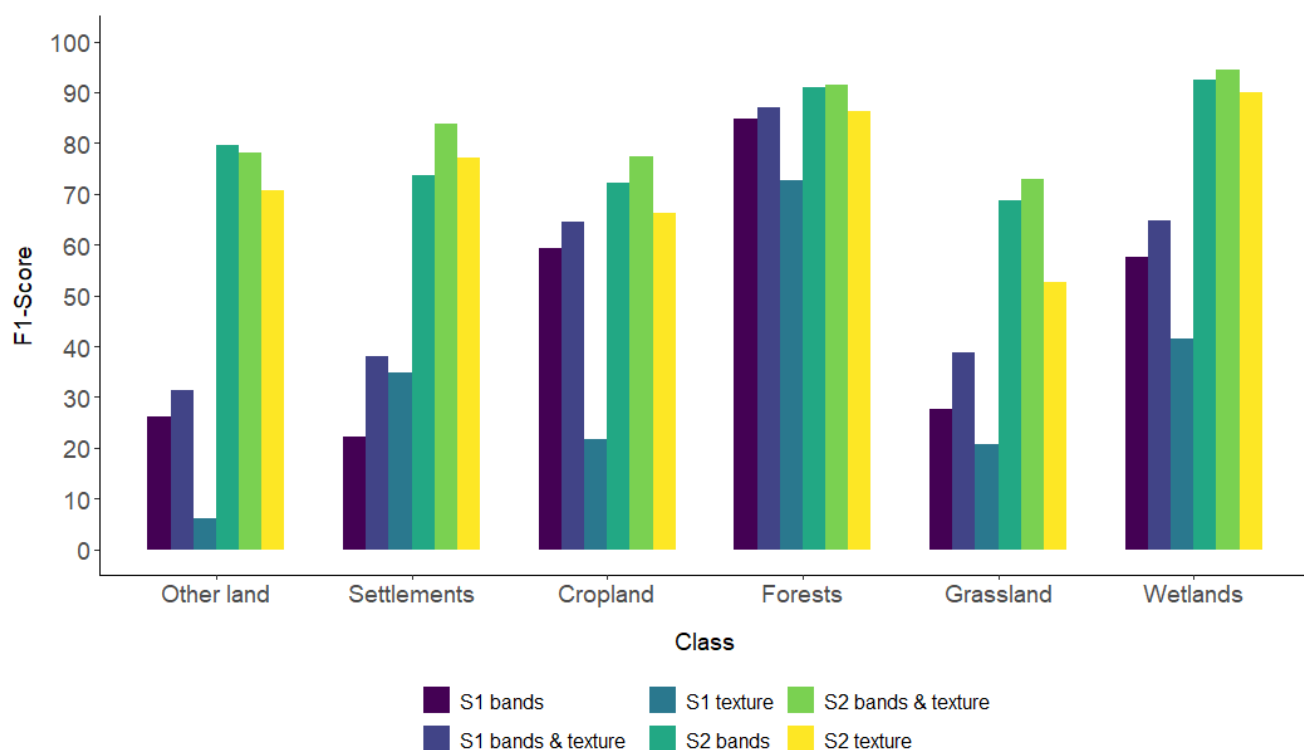


Fig. 4. Average F1- scores for IPCC classes comparing the S-1 and S-2 datasets.

3.2.3. Synergy of S-1 SAR and S-2 optical data for LULC mapping

As anticipated, the results showed that *combining* S-1 and S-2 increased the F1-score. The F1-score for forest land increased by 2-3% across the three seasons with the year-round images recording a 4% increase

when S-1 SAR was added to the S-2 optical data (See Supplementary Table S4). A similar pattern was observed for cropland with increments of 1%, 2%, 8% and 6% for the rainy (See Supplementary Table S1), dry (See Supplementary Table S2), hot (See Supplementary Table S3) and year-round (See Supplementary Table S4) images, respectively, when the S-1 bands were added to S-2 bands. An increment of 26% was observed in grassland mapping when S-1 year-round images were added to the S-2 year-round images. For the built-up class, a decline in F1-score was observed when S-1 and S-2 were combined for the rainy and hot seasons, while for the dry season and year-round images the F1-score increased. Other land showed minimal changes in F1-score, as for wetlands. This result indicates that the addition of S-1 SAR data to S-2 SAR data has different impacts on the different LULC classes and seasons. For example, we noted significant increases of 8% and 6% for cropland detection in the hot season and year-round image, respectively, and a 26% increase for grassland detection for the year-round images.

The highest F1-scores for each LULC class, for the time scales considered in this research, are shown in Table 4. Using multi-seasonal images produced higher F1-scores for forest, cropland and settlements while the other classes had similar or lower F1-scores to those obtained using the seasonal and annual images. Most studies that compared S-1 SAR data and S-2 optical data for LULC mapping or forest type mapping obtained similar overall accuracies, but none of the reviewed studies went deeper to compare the effects of S-1 and S-2 synergy on individual class F1-scores, except for Solórzano et al. (2021) who reported similar results to ours.

Table 4

F1-scores for seasonal, year-round, and multi-seasonal images for S-1 and S-2 combined.

	F1-score (%)				
	Rainy	Dry	Hot	Year-round	Multi-seasonal
Forests	94.9	92.6	92.9	94.3	95.7
Cropland	85.2	80.1	79.1	82.1	88.5
Grassland	89.5	87.4	73.1	93.4	92.6
Settlements	83.5	87.8	72.8	88.9	89.3
Other land	77.3	85.7	76.1	87.9	86.7
Wetlands	92.9	93.6	93.3	95.8	95.8

The highest overall accuracies and Kappa indices were obtained for the multi-seasonal case, as shown in Table 5. This result is consistent with previous research which suggested that incorporation of temporal images increases classification accuracy (Puletti et al., 2018; Ngo et al., 2020; Lopes et al., 2020). A statistical test at the 5% level of significance indicated no significant difference between the model accuracies for the seasonal images and year-round images (p -values of between 0.16 to 0.92). However, a significant difference was found between the individual seasonal images (and year-round image) and the multi-seasonal images (p -values of between 0.02 to 0.00).

Table 5

Overall accuracies and Kappa indices for seasonal, year-round and multi-seasonal S-1 and S-2 images combined.

	Rainy	Dry	Hot	Year-round	Multi-seasonal
Overall accuracy (%)	90.6	89.0	90.1	91.1	93.0
Kappa (%)	85.5	83.0	84.7	86.3	89.3

3.2.4. Visual Inspection

We inspected visually the LULC classified maps produced for a clip from our study area. The synergy of S-1 and S-2 produced the most visually pleasing and accurate map comparing favourably with the actual landscape (Fig. S7). The multi-seasonal map shows the LULC classes in greater detail (Fig. S8). The rainy season maps classified some grasslands as wetlands, which is to be expected given the spectral overlap between dambo grasslands (a shallow and seasonally wet grassy floodplain) and wetlands (refer to IPCC classification scheme; Shakachite et al., 2016)). A visual comparison of our most accurate LULC map (i.e., produced using multi-seasonal images) with the national forest map for 2014 (latest) produced under the ILUAII project and the 2019 Esri landcover map is shown in (Fig. 5). Our map identifies detailed LULC classes that are missed by both the ILUA and Esri maps. Note that although the ILUA map represents 2014, whereas our map and the Esri map represent 2019, the low quality of the map is visible. Quantitatively, our map achieved a higher overall accuracy; specifically, 93% compared to the ILUA map reported at 87.7% and Esri map reported at 85%.

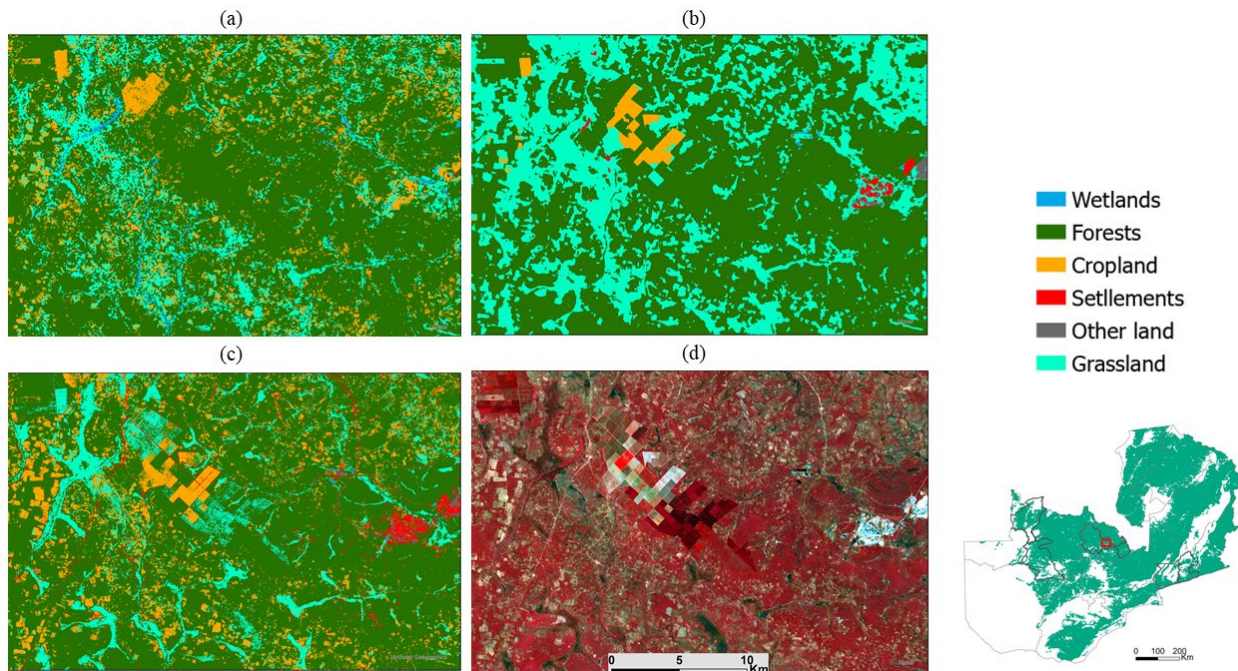


Fig. 5. Comparison of our best classified LULC map with two benchmark maps. (a), ILUA-2014 (b), Esri (c) this research, (d) S-2 colour infrared for comparison.

3.3. Forest type classification with U-net

The highest F1-score was achieved for the reference forest from the S-1+S-2 model followed by degraded forest and lastly for the regrowth forest using year-round images. The S-2 model had higher F1-scores than the S-1 model for all three forest type classes (Table 6). Only very small increases in F1-scores were achieved when S-1 and S-2 were combined.

We compared the commonly used spectral channels within the S-2 bands to assess their effect on model accuracy. Using the S-2 bands excluding the red edge bands (hereafter referred to as S-2–6 bands) produced greater overall accuracy and F1-scores for all three forest types compared to omitting the S-2 red edge bands

and shortwave infrared bands (hereafter, referred to as S-2–4 bands) (See Supplementary Table S5). Thus, using the S-2–10 bands (B2, B3, B4, B5, B6, B7, B8, B8A, SWIR1, SWIR2) produced greater accuracy than the S-2–4 bands, but excluding the red-edge bands had little effect on accuracy. This result differs from that of Ali and Johnson (2022) who concluded that the S-2–4 bands produced greater accuracy than the S-2–10 bands, although their classification was for the common LULC classes and not the forest types considered in this research. For the seasonal images, the S2 bands performed more accurately across all three seasons with the dry season images producing the highest accuracy (See Supplementary Tables S6 – S8). The S-1 bands produced the lowest accuracies for all three seasons.

Table. 6

F1-scores and Overall accuracy of forest types for S-1, S-2 and their combination for year-round images using the U-net algorithm.

Model	Classes	Precision (%)	Recall (%)	F1-score (%)	Overall Accuracy (%)
S-1 bands	Regrowth	36.5	30.8	33.4	45.4
	Degraded	48.8	31	37.9	
	Reference	47.5	72.3	57.3	
S-2 bands	Regrowth	71.1	68.3	69.6	75.6
	Degraded	70.5	69.2	69.9	
	Reference	82.1	86	84	
S-1 and S-2 bands	Regrowth	72.5	71.1	71.8	77.2
	Degraded	71.4	73.3	72.3	
	Reference	84.5	85	84.7	

When the most accurate models for each dataset (S-1+S-2, S-2 and S-1) were applied to the test datasets, the results followed a similar pattern to that of the training dataset with the S-1+S-2 bands producing the highest overall accuracy (See Supplementary Table S9) followed by the S-2 bands (See Supplementary Table S10), and lastly the S-1 bands (See Supplementary Table S11). Reference forest produced the highest user accuracy (81%) followed by the degraded (78%) and lastly regrowth (76%) classes.

We further analysed the results qualitatively by visually inspecting the produced maps. The S-1+S-2 bands produced a classified map that compared favourably with the three testing landscapes, clearly delineating reference forests (darker red in the colour infrared images), from degraded and regrowth forests. Closer analysis of the confusion matrices, and visual inspection, reveals that most mismatches occurred between degraded forests and regrowth forests, especially in landscapes with advanced degradation (i.e., the Copperbelt and Eastern province landscapes). This conforms with a similar observation by Ferrer et al. (2022). Classified images using the S-2 bands were almost as accurate as classified images using the S-1+S-2 bands in terms of mapping the three forest types (Table 6). Classified images using S-1 bands, consistent with the quantitative analysis, showed very low accuracy with no clear delineation of forest types (Fig. S9).

We compared the classification differences between the classified images produced using the RF and U-net algorithms. The U-net algorithm was found to be superior to the RF algorithm both in terms of quantitative accuracy and visual assessment (Fig. 6).

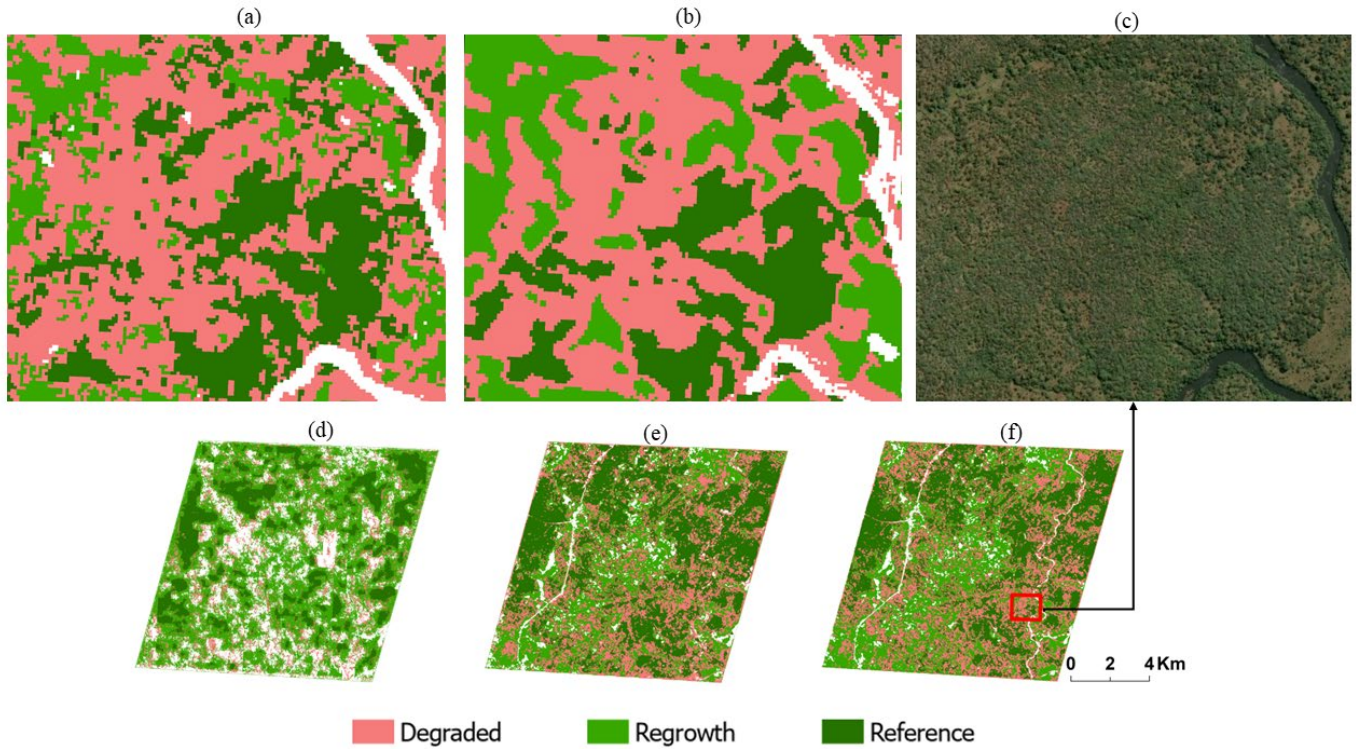


Fig. 6. Classified forest type maps for the North-western province test landscape for illustration. (a-c) a zoomed-in area comparing the RF and U-Net algorithms, (d-e) comparison of the different datasets using U-Net for a complete landscape tile. (a) RF, (b) U-net, (c) World View Image (29/12/2021), (d) S-1, (e), S-2 and (f) S1+S2.

4. Discussion

4.1. LULC mapping with RF in GEE

We explored the use of S-1 and S-2 data for LULC mapping of the Miombo woodlands using the RF algorithm in GEE. We compared bands, textures and their combination, as well as the effect of seasons, on mapping six IPCC classes (forests, cropland, grassland, settlements, wetlands, and other land). The results showed that the use of multi-seasonal images significantly increased LULC mapping accuracy for the Miombo woodlands. These findings agree with related studies (Higginbottom et al., 2018; de Souza Mendes et al., 2019; Lopes et al., 2020). Contrary to the view that dry season images produce higher accuracies for mapping Miombo woodlands (Kamusoko et al., 2014; Halperin et al., 2016; Ferrer Velasco et al., 2022), we found no significant difference in overall accuracy obtained by using either rainy or dry or hot season images or year-round images. Moreover, hot and rainy season images produced higher overall accuracies than dry season images. Studies that reported dry season images to be superior to rainy season images (Higginbottom et al., 2018; de Souza Mendes et al., 2019) considered forest types and woody cover and not the IPCC classification scheme used in this research. Our study considered three distinct seasons (rainy, dry and hot) unlike the two reviewed studies which considered only the rainy and dry seasons. We also found that S-1 bands combined with their textures performed well when mapping forests, a result confirmed by both quantitative and qualitative analysis.

When we compared our most accurate LULC map with secondary maps (i.e., the national LULC and the Esri landcover map), our map showed closer similarity to the actual landscape image than the two secondary maps (Figure 7). Forest areas in our map agreed spatially with both the Esri map and the ILUA map with small differences. A similar result was reported by Velasco et al. (2022) when they compared their classified

maps for tropical forests to global maps. However, we observed misclassifications for non-forest areas such as cropland and settlements. From visual inspection using Google Earth fine resolution imagery and Sentinel images, the Esri landcover map misclassified several croplands as rangeland, just as several settlements (built-up areas) were misclassified as rangeland. We recommend future studies are undertaken to scrutinise these discrepancies further, especially for the cropland and settlements classes, as these global LULC datasets are used for land accounting in developing countries such as Zambia where up-to-date locally calibrated LULC maps are not available (GRZ, 2022).

4.2. Forest type mapping with U-net

We used the U-Net CNN algorithm to map the three forest types (reference forests, degraded forests, regrowth forests) that characterise the Miombo woodlands. We hypothesised that U-Net can discriminate these spectrally similar forest types based on its ability to identify patterns in an image using both the spectral and spatial domains (Kattenborn et al., 2021). We trained U-Net models using different channels for the S-1 and S-2 bands. Our results showed that the U-net CNN can discriminate the three forest types especially when trained on a combination of S-1 and S-2 bands. Overall test accuracy increased by 5% when we added the S-1 bands to S-2 bands, which is a significant increase. These validation and test results form a basis on which further studies can be based aimed at increasing these accuracies further. Future research should explore other CNN methods which have been reported to produce high accuracies (Sharma et al., 2017; Brutzkus et al., 2022).

Reference forests were clearly delineated from degraded and regrowth forests, with the lowest F1-score of 78% for the S-2 bands from the rainy season and highest F1-score of 85% for the year-round S-1+ S-2 bands. This result is similar to that obtained by Solórzano et al. (2021) who reported an F1-score of 86% for old-growth forests. Prediction using the S-2 bands alone was almost as accurate as that using the S-1+S-2 bands for mapping reference forests. The small increase in F1-score when S-1 SAR data were combined with S-2 optical data shows that the SAR data do not contribute greatly to increasing the accuracy of the reference forest classification, contrary to expectations that the ability of SAR to interact with the vegetation canopy structure should help to increase accuracy. This result is similar to that reported elsewhere (de Souza Mendes et al., 2019; Lopes et al., 2020). The low contribution of S-1 SAR data towards increasing the F1-score for reference forest might be because the penetration of the C-band of S-1 in the dense canopies that characterise reference forests is limited, for example, compared to L-band or P-band which achieve greater penetration.

Very few studies attempted to discriminate forest types into degraded forests and regrowth forests. Most studies that tried to classify forest types for Miombo woodlands used forest parameters such as canopy cover to produce canopy cover classes and maps (Halperin et al., 2016; Verhegghen et al., 2022). Apart from the purposes of sound forest management practices, most of the methodologies for estimating and monitoring carbon emissions from forests such as the verified carbon standards (VCS) emphasise the need to delineate forests into distinguishable forest types to increase prediction accuracies. The need to classify forest types is, therefore, well-established. The overall objective of this research was to address this need by discriminating forest types using the state-of-the-art U-Net CNN. We obtained the highest F1-scores of 72% and 73% for regrowth and degraded forests, respectively, higher than the accuracies obtained by Solórzano et al. (2021) for regrowth forests. The training data for these two classes showed very close backscatter and spectral reflectance values. Our results demonstrate that regrowth forests and degraded forests can best be separated using the dry season images from S-2 bands and the year-round images from S-1+S-2 bands.

4.3. Hierarchical Approach for Mapping Miombo Woodland Forest Types

The hierarchical approach designed in this research, beginning with LULC mapping to delineate forest areas, and subsequently discriminating between the different forest types, was demonstrated to be effective in providing more accurate and detailed information about forest patterns compared to conventional methods. Discriminating between various LULC classes and forest types based on spectral and spatial characteristics can pose challenges for classification models, as certain classes closely resemble each other (Figure A1-A6).

For example, Solórzano et al. (2021) used a U-Net model to classify LULC, including distinguishing between different forest types among other classes, but achieved low classification accuracies due to the complexity of the classification system. On the other hand, de Souza Mendes et al. (2019) who adopted a similar forest masking approach before forest type classification, achieved favourable results using the RF algorithm for both classifications. In contrast, we utilised the state-of-the-art U-Net CNN for forest type mapping, demonstrating significant potential for identifying the complex patterns resulting from the fragmentation of Miombo vegetation structure and distribution. This research, therefore, addresses directly the specific challenge of mapping the sparse and heterogeneous Miombo woodlands into distinct forest types (reference, degraded, and regrowth) using satellite sensor and ground data. The mapping of Miombo woodlands into these forest classes holds considerable importance and can play a pivotal role in improving the accuracy of estimation of AGB, as well as supporting forest conservation initiatives, particularly those focused on restoring degraded and fragmented landscapes like the Transforming Landscapes for Resilience and Development (TRARD), as well as in forest carbon (biomass) projects such as REDD+ that are presently taking place within the Miombo woodlands.

5. Conclusion

This research aimed to explore the optimal combination of remotely sensed S-2 optical and S-1 SAR bands for mapping the dry tropical Miombo woodlands, which are of great significance, and which require monitoring and conservation. Specifically, we integrated mapping of *LULC* to identify the Miombo woodlands and then mapped *forest type* within the Miombo woodlands themselves. We used the RF algorithm executed in GEE for LULC mapping and the U-Net algorithm for forest type mapping, and both algorithms yielded promising results.

We assessed the influence of seasonal variation on classification accuracy and model performance by selecting the S-2 and S-1 images from specific seasons. Notably, the multi-seasonal image dataset produced the greatest accuracy for LULC classification. Further, we found that seasonal and year-round images did not exhibit statistically significant differences in terms of overall LULC classification accuracies. For mapping forest type, the year-round image dataset outperformed the others, with the dry season image producing the highest accuracy among the seasonal images.

The analysis revealed that the combination of S-2 and S-1 data increased the accuracy marginally for both LULC and forest type mapping, with S-2 optical data playing the dominant role. These results suggest the superiority of S-2 over S-1 for mapping Miombo woodlands in Africa.

In conclusion, the proposed hierarchical methodology, combining RF for forest mapping and U-Net for discriminating forest classes, was demonstrated to be effective and capable of generating accurate maps. The methodology can be readily adopted for Miombo woodland mapping and monitoring programs, offering valuable insights for Miombo biomass mapping and for conservation and land management efforts relating to this precious tropical dry woodland.

Author Contributions

KK conceived the idea and designed the methodology for the study supported by CZ and PMA. ML was involved in ground data collection through the Thünen Institute. KK analysed the data and drafted the manuscript with supervision from CZ and PMA. KK, CZ, ML and PMA critically reviewed the manuscript before giving approval for submission to the journal.

Acknowledgements

We thank the Commonwealth Scholarship Commission who provided funding for KK's Environmental Science doctoral training program at Lancaster University, PhD grant number: ZMCS-2021-536, for the period 2021 to 2024. We thank the Thünen Institute and CIFOR Zambia for providing the ground-validated data used in this research which were collected during the LaforeT project. We also thank Marco Vizzari for giving us access to the GEE script they developed for their study.

Declaration of competing interest

The authors declare that they have no known competing financial interests or personal relationships that could have appeared to influence the work reported in this paper.

Data Availability Statement

Ground data and remote sensing imagery together with codes used in this study will be made available upon request.

References

- (Grz), G. O. T. R. O. Z. (2022) Natural capital Accounts for Land, (2018-2021). National Remote Sensing Centre, Ministry of Lands and natural Resources and Ministry of Finance and National Planning.
- Adagbasa, E. G., Adelabu, S. A. & Okello, T. W. (2019) Application of deep learning with stratified K-fold for vegetation species discrimination in a protected mountainous region using Sentinel-2 image. *Geocarto international*, 1-21. 10.1080/10106049.2019.1704070.
- Ali, K. & Johnson, B. A. (2022) Land-Use and Land-Cover Classification in Semi-Arid Areas from Medium-Resolution Remote-Sensing Imagery: A Deep Learning Approach. *Sensors (Basel)*, 22(22), 8750. 10.3390/s22228750.
- Altarez, R. D. D., Apan, A. & Maraseni, T. (2023) Deep learning U-Net classification of Sentinel-1 and 2 fusions effectively demarcates tropical montane forest's deforestation. *Remote sensing applications*, 29, 100887. 10.1016/j.rsase.2022.100887.
- Bragagnolo, L., Da Silva, R. V. & Grzybowski, J. M. V. (2021) Amazon forest cover change mapping based on semantic segmentation by U-Nets. *Ecological informatics*, 62, 101279. 10.1016/j.ecoinf.2021.101279.
- Brandt, M., Wigneron, J.-P., Chave, J., Tagesson, T., Penuelas, J., Ciais, P., Rasmussen, K., Tian, F., Mbow, C., Al-Yaari, A., Rodriguez-Fernandez, N., Schurgers, G., Zhang, W., Chang, J., Kerr, Y., Verger, A., Tucker, C., Mialon, A., Rasmussen, L. V., Fan, L. & Fensholt, R. (2018) Satellite passive microwaves reveal recent climate-induced carbon losses in African drylands. *Nat Ecol Evol*, 2(5), 827-835. 10.1038/s41559-018-0530-6.
- Breiman, L. (2001) Random forests. *Machine learning*, 45(1), 5-32. 10.1023/A:1010933404324.
- Brutzkus, A., Globerson, A., Malach, E., Netser, A. R. & Shalev-Schwartz, S. (2022). *Efficient Learning of CNNs using Patch Based Features*. Unpublished paper presented at the Proceedings of the 39th International Conference on Machine Learning. Proceedings of Machine Learning Research.
- Carreiras, J. M. B., Jones, J., Lucas, R. M. & Shimabukuro, Y. E. (2017) Mapping major land cover types and retrieving the age of secondary forests in the Brazilian Amazon by combining single-date optical and radar remote sensing data. *Remote Sensing of Environment*, 194, 16-32. 10.1016/j.rse.2017.03.016.
- Connette, G., Oswald, P., Songer, M. & Leimgruber, P. (2016) Mapping distinct forest types improves overall forest identification based on multi-spectral landsat imagery for Myanmar's Tanintharyi Region. *Remote Sensing*, 8(11). 10.3390/rs8110882.
- Dal Molin, R. & Rizzoli, P. (2022) Potential of Convolutional Neural Networks for Forest Mapping Using Sentinel-1 Interferometric Short Time Series. *Remote sensing (Basel, Switzerland)*, 14(6), 1381. 10.3390/rs14061381.
- David, R. M., Rosser, N. J. & Donoghue, D. N. M. (2022) Remote sensing for monitoring tropical dryland forests: a review of current research, knowledge gaps and future directions for Southern Africa. *Environ. Res. Commun*, 4(4), 042001. 10.1088/2515-7620/ac5b84.
- Day, M., Gumbo, D., Moombe, K. B., Wijaya, A. & Sunderland, T. C. H. (2014) *Zambia country profile: Monitoring, reporting and verification for REDD+*. Center for International Forestry Research (CIFOR).

- De Souza Mendes, F., Baron, D., Gerold, G., Liesenberg, V. & Erasmi, S. (2019) Optical and SAR Remote Sensing Synergism for Mapping Vegetation Types in the Endangered Cerrado/Amazon Ecotone of Nova Mutum—Mato Grosso. *Remote sensing (Basel, Switzerland)*, 11(10), 1161. 10.3390/rs11101161.
- Decuyper, M., Chávez, R. O., Lohbeck, M., Lastra, J. A., Tsendbazar, N., Hackländer, J., Herold, M. & Vågen, T.-G. (2022) Continuous monitoring of forest change dynamics with satellite time series. *Remote Sensing of Environment*, 269, 112829. 10.1016/j.rse.2021.112829.
- Ferrer, V., Rubén Lippe, M., Günter, S., Jany, C., Mfuni, T., Rebuyas, R. S., Tamayo, F., Fischer, R., Eguiguren, P., Kazungu, M., Nansikombi, H., Ojeda-Luna, T. & Wiebe, P. (2023) LaForeT Ground control points and Landscape borders. Thünen Working Paper.
- Ferrer Velasco, R., Lippe, M., Tamayo, F., Mfuni, T., Sales-Come, R., Mangabat, C., Schneider, T. & Günter, S. (2022) Towards accurate mapping of forest in tropical landscapes: A comparison of datasets on how forest transition matters. *Remote sensing of environment*, 274. 10.1016/j.rse.2022.112997.
- Halperin, J., Lemay, V., Coops, N., Verchot, L., Marshall, P. & Lochhead, K. (2016) Canopy cover estimation in miombo woodlands of Zambia: Comparison of Landsat 8 OLI versus RapidEye imagery using parametric, nonparametric, and semiparametric methods. *Remote Sensing of Environment*, 179, 170-182. 10.1016/j.rse.2016.03.028.
- Hamedianfar, A., Mohamedou, C., Kangas, A. & Vauhkonen, J. (2022) Deep learning for forest inventory and planning: a critical review on the remote sensing approaches so far and prospects for further applications. *Forestry (London)*, 95(4), 451-465. 10.1093/forestry/cpac002.
- Higginbottom, T. P., Symeonakis, E., Meyer, H. & Van Der Linden, S. (2018) Mapping fractional woody cover in semi-arid savannahs using multi-seasonal composites from Landsat data. *ISPRS Journal of Photogrammetry and Remote Sensing*, 139, 88-102. 10.1016/j.isprsjprs.2018.02.010.
- Isaienkov, K., Yushchuk, M., Khramtsov, V. & Seliverstov, O. (2021) Deep Learning for Regular Change Detection in Ukrainian Forest Ecosystem With Sentinel-2. *IEEE Journal of Selected Topics in Applied Earth Observations and Remote Sensing*, 14, 364-376. 10.1109/JSTARS.2020.3034186.
- John, E., Bunting, P., Hardy, A., Silayo, D. S. & Masunga, E. (2021) A Forest Monitoring System for Tanzania. *Remote sensing (Basel, Switzerland)*, 13(16), 3081. 10.3390/rs13163081.
- Kamusoko, C., Gamba, J. & Murakami, H. (2014) Mapping woodland cover in the Miombo ecosystem: A comparison of machine learning classifiers. *Land (Basel)*, 3(2), 524-540. 10.3390/land3020524.
- Kattenborn, T., Leitloff, J., Schiefer, F. & Hinz, S. (2021) Review on Convolutional Neural Networks (CNN) in vegetation remote sensing. *ISPRS Journal of Photogrammetry and Remote Sensing*, 173, 24-49. 10.1016/j.isprsjprs.2020.12.010.
- Lopes, M., Frison, P. L., Durant, S. M., Schulte to Bühne, H., Ipavec, A., Lapeyre, V., Pettorelli, N. & Horning, N. (2020) Combining optical and radar satellite image time series to map natural vegetation: savannas as an example. *Remote Sensing in Ecology and Conservation*, 6(3), 316-326. 10.1002/rse2.139.
- Lu Zhang, X. W., Bing Sun TROPICAL NATURAL FOREST CLASSIFICATION USING TIME-SERIES SENTINEL-1 AND LANDSAT-8 IMAGES IN HAINAN ISLAND. *IGARSS 2019 - 2019 IEEE International Geoscience and Remote Sensing Symposium*. Yokohama, Japan. 6732–6735.
- Mayes, M. T., Mustard, J. F. & Melillo, J. M. (2015) Forest cover change in Miombo Woodlands: modeling land cover of African dry tropical forests with linear spectral mixture analysis. *Remote Sensing of Environment*, 165, 203-215. 10.1016/j.rse.2015.05.006.
- Mcnicol, I. M., Ryan, C. M. & Mitchard, E. T. A. (2018) Carbon losses from deforestation and widespread degradation offset by extensive growth in African woodlands. *Nat Commun*, 9(1), 3045-3045. 10.1038/s41467-018-05386-z.
- Mercier, A., Betbeder, J., Rumiano, F., Baudry, J., Gond, V., Blanc, L., Bourgoïn, C., Cornu, G., Ciudad, C., Marchamalo, M., Pocard-Chapuis, R. & Hubert-Moy, L. (2019) Evaluation of Sentinel-1 and 2

- Time Series for Land Cover Classification of Forest–Agriculture Mosaics in Temperate and Tropical Landscapes. *Remote sensing (Basel, Switzerland)*, 11(8), 979. 10.3390/rs11080979.
- Mudereri, B. T., Chitata, T., Mukanga, C., Mupfiga, E. T., Gwatirisa, C. & Dube, T. (2021) Can biophysical parameters derived from Sentinel-2 space-borne sensor improve land cover characterisation in semi-arid regions? *Geocarto international*, 36(19), 2204-2223. 10.1080/10106049.2019.1695956.
- Ngo, K. D., Lechner, A. M. & Vu, T. T. (2020) Land cover mapping of the Mekong Delta to support natural resource management with multi-temporal Sentinel-1A synthetic aperture radar imagery. *Remote sensing applications*, 17, 100272. 10.1016/j.rsase.2019.100272.
- Nicolau, A. P., Flores-Anderson, A., Griffin, R., Herndon, K. & Meyer, F. J. (2021) Assessing SAR C-band data to effectively distinguish modified land uses in a heavily disturbed Amazon forest. *International Journal of Applied Earth Observation and Geoinformation*, 94, 102214. 10.1016/j.jag.2020.102214.
- Numbisi, F. N., Van Coillie, F. M. B. & De Wulf, R. (2019) Delineation of Cocoa Agroforests Using Multiseason Sentinel-1 SAR Images: A Low Grey Level Range Reduces Uncertainties in GLCM Texture-Based Mapping. *ISPRS international journal of geo-information*, 8(4), 179. 10.3390/ijgi8040179.
- Phiri, D., Morgenroth, J., Xu, C. & Hermosilla, T. (2018) Effects of pre-processing methods on Landsat OLI-8 land cover classification using OBIA and random forests classifier. *International Journal of Applied Earth Observation and Geoinformation*, 73, 170-178. 10.1016/j.jag.2018.06.014.
- Praticò, S., Solano, F., Di Fazio, S. & Modica, G. (2021) Machine learning classification of mediterranean forest habitats in google earth engine based on seasonal sentinel-2 time-series and input image composition optimisation. *Remote sensing (Basel, Switzerland)*, 13(4), 1-28. 10.3390/rs13040586.
- Prudente, V. H. R., Sanches, I. D., Adami, M., Skakun, S., Oldoni, L. V., Xaud, H. a. M., Xaud, M. R. & Zhang, Y. SAR Data for Land Use Land Cover Classification in a Tropical Region with Frequent Cloud Cover. *International Geoscience and Remote Sensing Symposium (IGARSS)*. 4100-4103.
- Puletti, N., Chianucci, F. & Castaldi, C. (2018) Use of Sentinel-2 for forest classification in Mediterranean environments. *Annals of Silvicultural Research*, 42(1), 32-38. 10.12899/ASR-1463.
- Ribeiro, N., Cumbana, M., Mamugy, F. & Chaúque, A. (2012) Remote Sensing of Biomass in the Miombo Woodlands of Southern Africa: Opportunities and Limitations for Research. *Remote Sensing of Biomass - Principles and Applications*. Lola Fatoyinbo ed. Croatia: InTech:Rijeka.
- Romijn, E., Lantican, C. B., Herold, M., Lindquist, E., Ochieng, R., Wijaya, A., Murdiyarso, D. & Verchot, L. (2015) Assessing change in national forest monitoring capacities of 99 tropical countries. *Forest ecology and management*, 352, 109-123. 10.1016/j.foreco.2015.06.003.
- Shakachite, O., Chungu, D., Ng'andwe, P., Siampale, A. M., Chendauka, B., Vesa, L. & Roberts, W. J. (2016) Integrated Land Use Assessment II – Report for Zambia. The Food and Agriculture Organization of the United Nations and the Forestry Department, Ministry of Lands and Natural Resources, Lusaka, Zambia.
- Shamaoma, H., Chirwa, P. W., Ramoelo, A., Hudak, A. T. & Syampungani, S. (2022) The Application of UASs in Forest Management and Monitoring: Challenges and Opportunities for Use in the Miombo Woodland. *Forests*, 13(11), 1812. 10.3390/f13111812.
- Sharma, A., Liu, X., Yang, X. & Shi, D. (2017) A patch-based convolutional neural network for remote sensing image classification. *Neural Netw*, 95, 19-28. 10.1016/j.neunet.2017.07.017.
- Solórzano, J. V., Mas, J. F., Gao, Y. & Gallardo-Cruz, J. A. (2021) Land use land cover classification with U-net: Advantages of combining sentinel-1 and sentinel-2 imagery. *Remote sensing (Basel, Switzerland)*, 13(18), 3600. 10.3390/rs13183600.
- Tassi, A., Gigante, D., Modica, G., Di Martino, L. & Vizzari, M. (2021) Pixel-vs. Object-based landsat 8 data classification in google earth engine using random forest: The case study of maiella national park. *Remote sensing (Basel, Switzerland)*, 13(12), 2299. 10.3390/rs13122299.

- Tsai, Y. H., Stow, D., Chen, H. L., Lewison, R., An, L. & Shi, L. (2018) Mapping vegetation and land use types in Fanjingshan National Nature Reserve using google earth engine. *Remote sensing (Basel, Switzerland)*, 10(6), 927. 10.3390/rs10060927.
- Verhegghen, A., Kuzelova, K., Syrris, V., Eva, H. & Achard, F. (2022) Mapping Canopy Cover in African Dry Forests from the Combined Use of Sentinel-1 and Sentinel-2 Data: Application to Tanzania for the Year 2018. *Remote Sensing*, 14(6). 10.3390/rs14061522.
- Vizzari, M. (2022) PlanetScope, Sentinel-2, and Sentinel-1 Data Integration for Object-Based Land Cover Classification in Google Earth Engine. *Remote sensing (Basel, Switzerland)*, 14(11), 2628. 10.3390/rs14112628.
- Wagner, F. H., Sanchez, A., Tarabalka, Y., Lotte, R. G., Ferreira, M. P., Aidar, M. P. M., Gloor, E., Phillips, O. L., Aragão, L. E. O. C., Pettorelli, N. & Clerici, N. (2019) Using the U-net convolutional network to map forest types and disturbance in the Atlantic rainforest with very high resolution images. *Remote Sensing in Ecology and Conservation*, 5(4), 360-375. 10.1002/rse2.111.